Research article

Frédéric Peyskens[a], Pieter Wuytens[a,*], Ali Raza, Pol Van Dorpe and Roel Baets

Waveguide excitation and collection of surface-enhanced Raman scattering from a single plasmonic antenna

https://doi.org/10.1515/nanoph-2018-0003
Received January 5, 2018; revised February 2, 2018; accepted February 3, 2018

Abstract: The integration of plasmonic antennas on single-mode silicon nitride waveguides offers great perspective for integrated surface-enhanced Raman spectroscopy (SERS). However, the few reported experimental demonstrations still require multiple plasmonic antennas to obtain a detectable SERS spectrum. Here, we show, for the first time, SERS signal detection by a single nanoplasmonic antenna integrated on a single-mode SiN waveguide. For this purpose, we investigated a backscattering detection scheme in combination with background noise reduction, which allowed an optimization of the signal-to-noise ratio (SNR) of this platform. Furthermore, a comparison with the free-space SERS spectrum of the same antenna shows that the conversion efficiency from pump power to total radiated Stokes power is twice as efficient in the case of waveguide excitation. As such, we explored several important aspects in the optimization of on-chip SERS sensors and experimentally demonstrated the power of exciting nanoplasmonic antennas using the evanescent field of a waveguide. This observation not only is useful for Raman sensing but also could be beneficial for any process involving plasmonic enhancement.

Keywords: integrated photonics; plasmonics; surface-enhanced Raman spectroscopy.

[a]**Frédéric Peyskens and Pieter Wuytens:** These authors contributed equally to this work.
***Corresponding author: Pieter Wuytens,** Photonics Research Group, INTEC Department, Ghent University-IMEC, Technologiepark-Zwijnaarde 15, 9052 Ghent, Belgium; Center for Nano- and BioPhotonics, Technologiepark-Zwijnaarde 15, 9052 Ghent, Belgium, e-mail: pieter.wuytens@ugent.be. http://orcid.org/0000-0002-0793-256X
Frédéric Peyskens: Photonics Research Group, INTEC Department, Ghent University-IMEC, Technologiepark-Zwijnaarde 15, 9052 Ghent, Belgium; Center for Nano- and BioPhotonics, Technologiepark-Zwijnaarde 15, 9052 Ghent, Belgium; and Quantum Photonics Group, RLE, Massachusetts Institute of Technology, 77 Massachusetts Avenue, Cambridge, MA 02139, USA
Ali Raza and Roel Baets: Photonics Research Group, INTEC Department, Ghent University-IMEC, Technologiepark-Zwijnaarde 15, 9052 Ghent, Belgium; and Center for Nano- and BioPhotonics, Technologiepark-Zwijnaarde 15, 9052 Ghent, Belgium
Pol Van Dorpe: IMEC, Kapeldreef 75, 3001 Heverlee, Belgium; and Department of Physics, KULeuven, Celestijnenlaan 200D, 3001 Leuven, Belgium

1 Introduction

The fingerprint specificity of Raman spectroscopy could make it an ideal identification or imaging technique for a plethora of applications. However, most molecules have a very small Raman cross-section, resulting in extremely weak signals. Methods for enhancing these weak Raman signals have seen a tremendous progress over the last decades, typically based either on nonlinear Raman scattering processes, such as coherent anti-Stokes and stimulated Raman scattering [1, 2], or on a strong local field enhancement, such as surface-enhanced Raman scattering [3–15] using either metals or dielectrics [16]. More recently, alternative geometries to the conventional microscope-based setup have been developed for collecting an increased amount of Raman scattering, such as hollow-core photonic crystal fibers [17] and nanophotonic waveguides on photonic integrated circuits (PICs) [18–21]. The latter make use of the strong evanescent field on the surface of nanophotonic waveguides to efficiently excite and collect Raman scattering of molecules in the vicinity of the waveguide. Due to the long interaction length along the waveguide, waveguide-enhanced Raman can collect 10–100 times more Raman signal as compared with conventional, free-space systems [18]. A hybrid integration of plasmonic nano-antennas with dielectric nanophotonic waveguides furthermore enabled waveguide-based excitation [22, 23] and collection of SERS spectra [24–27]. This approach holds the perspective of bringing the sensitivity and selectivity of SERS measurements to a fully integrated lab-on-a-chip. Technological developments over the last

decades have led to a continuing improvement of both the sensitivity and the reproducibility of free-space SERS substrates [9, 12, 13], up to the limit of single-molecule detection on top-down fabricated nano-antennas [28]. In contrast, the sensitivity of current waveguide-based SERS systems is still far away from the single-molecule detection limit. To date, even multiple gold structures are needed to achieve a detectable SERS signal [24]. On one hand, this limited sensitivity is due to technological and conceptual challenges related to the hybrid integration of gold nano-antennas on single-mode dielectric photonic waveguides, complicating the fabrication of superior geometries with nanometer-sized gaps. On the other hand, background Stokes scattering from the waveguide material itself will be superimposed on the SERS signal, limiting the signal-to-noise ratio (SNR) through shot noise [29]. In contrast to conventional waveguide-based Raman, absorption of the plasmonic structures limits the signal gain when increasing the waveguide length.

In this manuscript, we show, for the first time, SERS signal detection from a single nanoplasmonic antenna integrated on a single-mode silicon nitride (SiN) waveguide. For this purpose, we investigated both numerically and experimentally how the length of the access waveguide and number of plasmonic antennas influence the SNR in a backscattering detection scheme. Furthermore, we quantitatively compare the Stokes power from a single antenna collected through the waveguide to a free-space excitation and collection of the same antenna using a high numerical aperture (NA) objective. We also numerically investigated the differences in total excited Stokes scattering and collection efficiency of this Stokes scattered power in both geometries. While in both cases, an approximately equal amount of SERS scattered light is collected for a given input power, we find that the conversion efficiency from pump power to total radiated Stokes power is twice as high using waveguide-based excitation. The results described in this paper take a next step towards a sensitive integrated SERS platform and provide valuable insight for the development of future waveguide-based plasmonic sensors.

2 Results

Gold bowtie antennas were patterned on single-mode silicon nitride waveguides according to a previously reported method [24]. Figure 1A shows an exemplary scanning electron microscopy image of such a bowtie-patterned waveguide. Two sets of waveguides were fabricated and characterized. The first one has an increasing number of bowties on each waveguide, with a length of 400 µm between the input facet of the chip and the bowtie section and a separation of 1 µm between consecutive bowties. A second set consists of single bowties on waveguides with a length increasing from 20 µm to 520 µm. Both sets will be described further in this manuscript. We repeatedly managed to fabricate these bowtie-patterned waveguides; however, there are a number of fabrication imperfections during the two-step electron beam lithography. The two most prominent effects can be seen from Figure 1A. First, there is a consistent misalignment of 174 ± 3 nm between the center of the waveguide and the center of the bowties due to mechanical drift in the electron beam. Furthermore, close-ups of eight randomly selected bowties

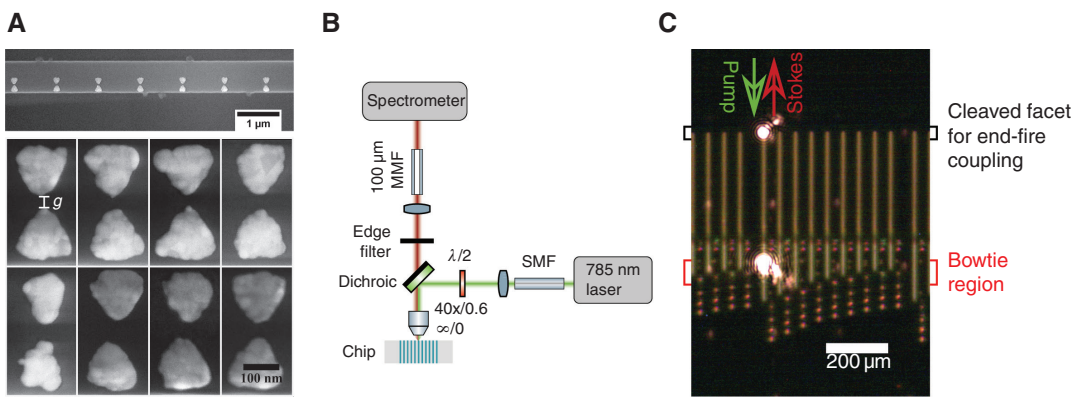

Figure 1: Waveguide geometry and optical coupling scheme.
(A) Scanning electron microscopy image of an array of bowties patterned on a waveguide and close-ups of eight different bowtie antennas, with a gap *g* in between the two triangles of 37 ± 9 nm. (B) The chip is placed vertically under a confocal Raman microscope and end-fire coupled with a 785-nm pump laser. Stokes scattered light is collected in reflection through the same objective. (C) Camera image of the chip installed under the Raman microscope. Scattering of the pump light is visible at the entrance facet of the chip and the bowtie-patterned region.

show some heterogeneity between the different structures, having a gap g of 37 ± 9 nm, height of 138 ± 5 nm, and width of 140 ± 15 nm. These variations have only a limited influence on both the field intensity in the gap and the spectral properties of the localized surface plasmon polariton. These effects were simulated through three-dimensional (3D) FDTD and described in more detail in the Supplementary Information (SI). In future, a reduction of the fabrication variations could be possible through an in-depth process optimization or the use of techniques to directly pattern nanostructures on topographical samples with nanometer resolution such as induced-deposition mask lithography [30]. After fabrication, the gold bowties were labeled with para-nitrothiophenol (pNTP), after which SERS spectra were excited and collected through the waveguide in an end-fire coupled reflection measurement, as depicted in Figure 1B and C, described in detail in the Methods section.

We first consider the dependence of the pNTP signal on the number of antennas (N) in a backscattering configuration. The antenna attenuates the power at the pump wavelength (λ_P = 785 nm) and Stokes wavelength (λ_S) with respective linear extinction coefficients e_p and e_S. As a consequence, the first antenna will feel the highest excitation power. Moreover, the SERS signal generated by antenna n (n = 1…N) still has to propagate back along the previous n–1 antennas. As a result, the overall SERS signal is expected to saturate for a sufficiently large N as the first antenna will always contribute the most, while the signal from subsequent antennas will exponentially decrease. If a single antenna generates $P_A = \eta_A(\lambda_P, \lambda_S)P_{\text{pump}}$ guided Stokes power for a given guided input power P_{pump}, the overall backscattered SERS signal P^R_{tot} for a given pump power at the input facet of a dielectric waveguide with length L and propagation loss α_{wg} is given by (See SI):

$$\frac{P^R_{\text{tot}}}{P_{\text{pump}}} \approx \eta_A(\lambda_P, \lambda_S) e^{-2L\alpha_{wg}} \left(\frac{1-\left(\frac{1}{e_P e_S}\right)^N}{1-\left(\frac{1}{e_P e_S}\right)} \right) \approx \text{FOM}_R(N, \lambda_P, \lambda_S) e^{-2\alpha_{wg}L} \quad (1)$$

Here, FOM_R represents the Raman conversion efficiency of N antennas, independent of the propagation loss of the waveguide. Figure 2A shows the backscattered Raman spectra for a set of waveguides with fixed length from the input facet to the first antenna with a varying number of antennas. The peaks associated to pNTP are highlighted with red (1080 cm^{-1}), green (1110 cm^{-1}), cyan (1340 cm^{-1}), and blue (1575 cm^{-1}). The characteristic SiN peak, originating from propagation of the mode through 400 µm of waveguide, is highlighted in orange (2330 cm^{-1}). For a single antenna (N=1), the overall SiN Raman background is still too high to resolve all pNTP peaks. Only the dominant 1340 cm^{-1} peak is visible. By increasing the number of antennas, all pNTP peaks become visible. Figure 2B shows the (background subtracted) SERS signal strength of the 1340-cm^{-1} peak as a function of N. Here, the pNTP peaks are normalized with respect to the SiN peak in order to compensate for minor differences in waveguide loss and edge-coupling efficiency among the waveguides. The solid blue line shows a fit of the analytical model in equation (1) to the experimental data. From this fit, we derive $\frac{1}{e_P e_S} = 0.79$, corresponding to an optical loss of 1.02 dB per antenna, and a single antenna conversion efficiency η_A of 4.55e^{-12} (see SI for the conversion between signal counts and FOM_R). The expected saturation trend with increasing number of antennas is clearly visible. However, as was shown in Figure 1A, not every antenna in the array will be the same due to fabrication

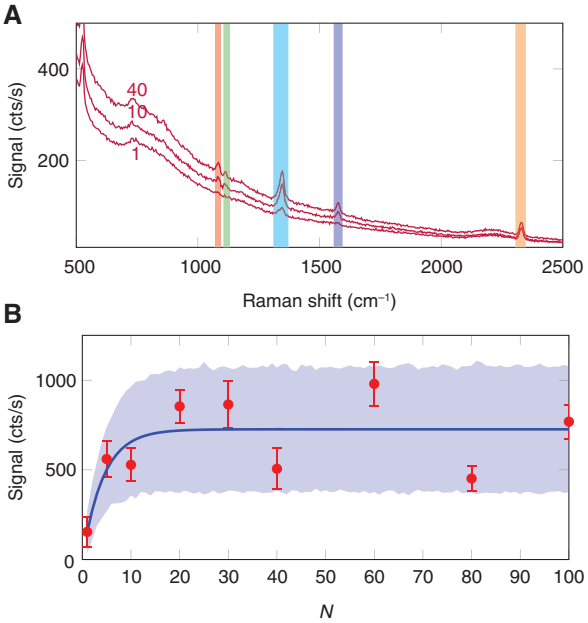

Figure 2: Waveguide-excited SERS signals for varying number of antennas.
(A) Backscattered Raman spectra of a waveguide covered with N = 1, 10 and 40 antennas. The red (1080 cm^{-1}), green (1110 cm^{-1}), cyan (1340 cm^{-1}), and blue (1575 cm^{-1}) lines correspond to pNTP peaks [24], while the orange peak (2330 cm^{-1}) is associated to the SiN [18]. (B) Backscattered SERS signal of the 1340 cm^{-1} peak as a function of N. The solid blue line represents a fit to the ideal model, while the shaded area represents the signal counts probability distribution due to differences in antenna conversion efficiency or extinction.

variations. This results in a variation on the signal counts. In particular, variations on the gap g of the first antennas on the waveguide will effect P_{tot}^{R}. In order to account for this spread, we apply a randomized fit procedure where a normal distribution for $\frac{1}{e_P e_S}$ and η_A will generate a signal count distribution. For more details on this procedure, we refer to our earlier work [24]. The blue shaded area in Figure 2B covers all datapoints and is generated using normal distributions for $\frac{1}{e_P e_S} = 0.79 \pm 0.08$ and $\eta_A = (4.55 \pm 1.20) \times 10^{-12}$. Based on numerical simulations with Lumerical FDTD Solutions (see SI), we calculated the theoretical value of $\frac{1}{e_P e_S} = 0.80$ and $\eta_A = 1.11 \times 10^{-13}$ for the studied antenna geometry ($L = 138$ nm, $g = 39$ nm, $\alpha = 60°$). Remarkably, the experimental η_A value is strongly underestimated by the simulation. This could be due to a variety of reasons. One reason is that a chemical enhancement factor could also contribute to the overall Raman signal [31]. These possible "chemical" changes to the polarizability of pNTP upon gold-binding are not incorporated in our model, which is purely based on electromagnetic enhancement mechanisms. Furthermore, the thickness of the Ti adhesion layer plays an important role, as a decrease of the Ti thickness can increase the SERS intensity by one order of magnitude [32]. Despite the discrepancy in the absolute signal strength, it is clear that the experimental data correlate with the predicted trend for on-chip backscattered SERS sensing [33]. The signal of the first antenna, which is the strongest, is fully available at the input facet for the backscattered light, while in the forward scattering direction, it is attenuated by the subsequent antennas in the array. Hence, the backscattered signal will never be smaller than the forward scattered signal, such that the suggested formula for the backscattered Raman signal represents the maximum achievable electromagnetic SERS enhancement $S_{max} = \eta_A \frac{e_P e_S}{e_P e_S - 1}$ as a function of the geometrically tunable antenna parameters. As such, the experimental demonstration of backscattering detection and its fit to our model is an important step to optimize the detection limit of an on-chip SERS platform by maximizing the absolute signal strength.

Nevertheless, we see that even with this backscattering configuration, some signal peaks are still too small to be detected using a single antenna. The main reason for this is the SiN background, which can be mitigated by decreasing the propagation length along the waveguide. For that purpose, we studied the SNR as a function of waveguide length L between the input facet and a single bowtie antenna patterned on the waveguide. Figure 3A shows the Raman spectra of a waveguide functionalized with $N = 1$ antenna, whereby the shortest length L between the input facet and the antenna equals 50 µm. Figure 3B shows the corresponding SNR for all pNTP peaks as a function of length L. For $L < L_1^c = 175$ µm, all pNTP peaks are visible in the spectrum, which is evidenced by an SNR ≥ 1. This is the first experimental demonstration of broadband on-chip SERS detection (as now all peaks are resolved) using a single nanoplasmonic antenna integrated on a

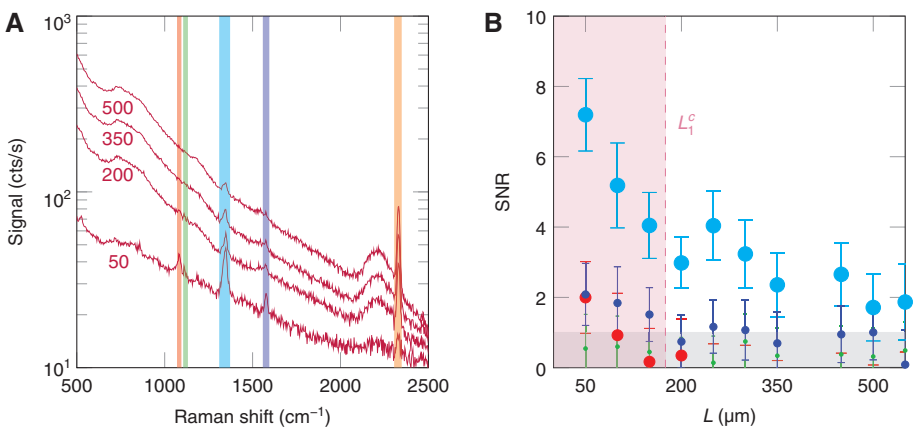

Figure 3: SiN Raman background with increasing length of the access waveguide.
(A) Backscattered Raman spectra of a waveguide covered with $N = 1$ antenna and varying length $L = 50 \ldots 500$ m. The lengths L are mentioned next to their corresponding Raman spectra, and the color codes for the lines are the same as in Figure 1. (B) SNR of all peaks for $N = 1$. Each color corresponds to the respective peak in the Raman spectrum. The grey shaded area represents SNR <1 and hence marks a region where detection is impossible. The purple shaded area represents the region where all peaks have an SNR >1.

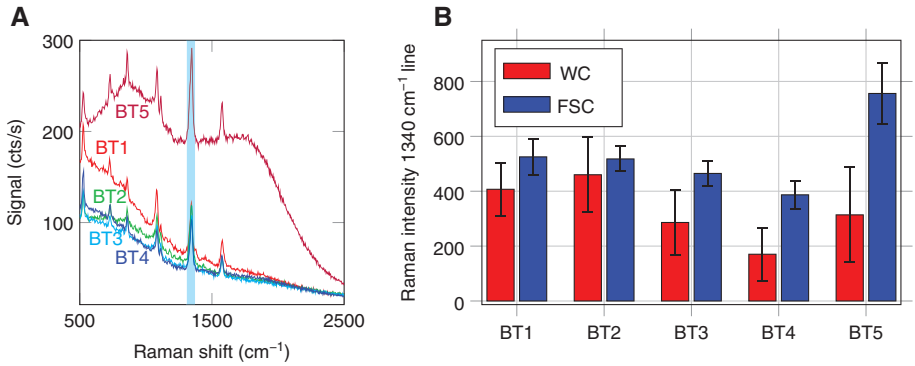

Figure 4: Free-space versus waveguide-excited single-antenna SERS spectra.
(A) Raman spectra from five different waveguides with $N=1$ antenna on top (BT1, …, BT5), but now the SERS signal from the antenna is excited and collected using a top-down configuration and not through the waveguide. (B) Comparison between the SERS signal of the 1340 cm^{-1} peak, excited and collected through the waveguide (WC) and through the objective (FSC). The signal values of the FSC measurements were re-scaled to normalize them with respect to the excitation power of the waveguide measurement.

single-mode SiN waveguide. More information on the analytical prediction of the SNR as well as a comparison with spontaneous on-chip Raman scattering can be found in the SI. As can be seen from Figure 3A, the SiN background is still present for a 50-µm short access waveguide. This shows that a sensitive waveguide-based SERS system requires to limit the length over which Raman signals are collected to tens of micrometers.

Finally, we make a quantitative comparison of the conversion efficiency from pump power to collected Stokes scattered power on identical single bowtie antennas obtained through waveguide excitation and collection (waveguide coupled, WC) versus excitation and collection through a conventional microscope objective (free-space coupled, FSC). In both cases, the polarization of the pump laser was aligned parallel to the gap of a specific bowtie on top of a SiN waveguide. The excitation at the entrance facet of the objective was 0.5 mW for the WC measurement and 0.15 mW for the FSC measurement. This lower power was chosen to avoid reduction of pNTP into dimercaptoazobenzene [34]. To allow for a fair comparison, the SERS intensities were scaled for equal excitation power, incorporating a 9.1-dB coupling loss (see SI) for end-fire coupling the light in and out of the single-mode waveguide. The Raman spectra of the FSC measurements are shown in Figure 4A, while the comparison is shown in Figure 4B. Note that small variations among the different bowties (e.g. changes in height or gap) give rise to different absolute signal strengths. Deviations in the ratio between WC and FSC can additionally be attributed to variations in the waveguide or coupling loss. From a comparison of five different bowties, shown in Figure 4B, we find that for the same excitation power, waveguide-based excitation and collection results in a collected Stokes scattered power that is 62±20% of that using a 0.9 NA objective. While these experimental data show the overall conversion from pump power to collected Stokes power, both the excitation of the localized surface plasmon resonance and the collection of Stokes scattered light have a different efficiency in the waveguide-coupled case as compared to the FSC measurement. Therefore, it is of interest to compare the efficiency by which the total radiated Stokes power is collected by either the objective (FSC) or the waveguide (WC). The collected Stokes power P_c^{WC} into the fundamental backward propagating mode is given by $P_c^{WC}=\beta_{WC}P_{\text{rad}}^{WC}$, where β_{WC} is the collection efficiency into the backward propagating mode and P_{rad}^{WC} is the total radiated power in the case of waveguide-coupled excitation. The conversion efficiency of pump power to Stokes scattered power ξ_c^{WC} is determined by $\xi_c^{WC}=P_{\text{rad}}^{WC}/P_{\text{pump}}$. In a similar way, we can write this down for the FSC case, $P_c^{\text{FSC}}=\beta_{\text{FSC}}P_{\text{rad}}^{\text{FSC}}$ and $\xi_c^{\text{FSC}}=P_{\text{rad}}^{\text{FSC}}/P_{\text{pump}}$, where the same excitation power P_{pump} as for the WC case is used. From the data in Figure 4B, we derived that for the same excitation power, the collected Stokes power $P_c^{WC}=(0.62\pm0.2)\times P_c^{\text{FSC}}$, such that $\xi_c^{WC}\approx 0.62\,\frac{\beta_{\text{FSC}}}{\beta_{WC}}\xi_c^{\text{FSC}}$. The overall conversion efficiency from pump to Stokes power for the WC case is hence $0.62\,\frac{\beta_{\text{FSC}}}{\beta_{WC}}$, more efficient compared to the FSC case. In order to assess β_{FSC} and β_{WC}, we simulated a radiating dipole source in the center of the gap of a bowtie antenna ($L=133$ nm, $\Delta=37$ nm, rad and an offset of 172 nm with respect to the center of the waveguide) and calculated the mode-coupled power and the power radiated within a numerical aperture of NA = 0.9. Based on these calculations, we estimate $\beta_{\text{FSC}}\approx 15.2\%$ and $\beta_{WC}\approx 5.5\%$ at 1340 cm^{-1}. As such, edge coupled excitation is about two times more efficient

than top down excitation using a 0.9-NA objective, at least for this particular geometry.

3 Conclusion

In conclusion, we showed SERS signal detection by a single nanoplasmonic antenna integrated on a single-mode SiN waveguide and investigated how the performance of a single integrated antenna compares to the performance of an identical, free-space excited, antenna. We found that the overall conversion efficiency from pump power to total radiated Stokes is twice as large as compared free-space excitation with a high NA (0.9) objective; however, a lower collection efficiency implies that the total amount of collected Stokes power is comparable in both systems. In order to obtain single antenna signal detection, we implemented a backscattering detection scheme in combination with background noise reduction, which allowed an optimization of the SNR of this platform. At waveguide lengths above 50 μm, the SNR of the system is clearly limited by the SiN background signal. In the future, a further increase in sensitivity could be achieved from a further reduction of the access waveguide length to a few micrometers or an increase of the plasmonic enhancement of the nanoantennas. An important asset of an integrated antenna is that it can always be aligned by fabrication with the ideal polarization, easing optimal excitation and stability. Combined with an integrated laser source and detector, an on-chip SERS probe could hence outperform traditional SERS sensing and provide a potentially more efficient platform for Raman sensing. Our results highlight several important aspects in the optimization of on-chip SERS sensors and, moreover, experimentally show the strength of exciting nanoplasmonic antennas using the evanescent field of a waveguide as opposed to free-space excitation. The latter observation is not only useful for Raman sensing but also could be beneficial for any process involving plasmonic enhancement, such as fluorescence enhancement of two-dimensional materials [35], nonlinear optics [36], and quantum optics [37].

4 Methods

4.1 Fabrication of bowtie-patterned waveguides

The fabrication process is similar to that described in our earlier work [24]. Briefly, the device is fabricated using a two e-beam lithographic steps. In the first step, gold nanoantennas are patterned on a $Si/SiO_2/SiN$ slab. PMMA resist (3% chlorobenzene) is used for 2 nm Ti/30 nm Au lift-off. The Ti/Au layer is deposited in a Pfeiffer Spider sputter system. In the second step, the SiN waveguides are defined. After metal lift-off, ma-N 2405 resist is spin-coated, exposed, and developed in ma-D 525. To avoid charging effects, a thin layer of e-spacer is also spun on top of the ma-N 2405. The developed samples are then etched with an ICP plasma (C4F8/SF6 mixture) in a commercial Oxford Plasmalab system. The resist is stripped with mr-Rem 700. Scanning electron microscope images were acquired on a FEI Nova 600 Nanolab Dual-Beam FIB system, using a voltage of 18 kV and a through the lens (TLD) detection.

4.2 Surface functionalization

The chip was labeled with para-nitrothiophenol (pNTP, Sigma), which selectively binds through the gold surface through a gold-thiol bond and serves as a model molecule for quantifying the surface enhancement. To this end, the chips were first cleaned with aceton and IPA and dried with a nitrogen gun. Next, a short O_2 plasma (PVA-TEPLA GIGAbatch 310 M, 6000 sccm O2, 600 W, 750 mTorr) was applied to further remove contaminants and render the gold surface hydrophilic. Subsequently, the chips were immersed in a 1-mM pNTP solution in ethanol. After overnight labeling, excess molecules were washed out by rinsing the chip extensively with ethanol and water.

4.3 SERS measurements

A commercial confocal Raman microscope (WITEC Alpha300R+) was used for coupling the light in and out of the chip, which is positioned vertically and end-fire coupled, as shown in Figure 1B and C. The same microscope was used for collecting a conventional free-space excited and collected SERS spectrum on the same bowties, which allowed for an accurate comparison between both. A 785-nm excitation diode laser (Toptica XTRA II) was used for excitation. The polarization of the excitation beam was set to be in line with the long axis of the bowties, which corresponded to the TE mode when using waveguide-based excitation. A laser power of 0.5 mW (waveguide coupled) or 0.15 mW (free space) was measured at the entrance facet of a Zeiss 100x/0.9 EC Epiplan NEOFLUAR; ∞/0 objective. The scattered signal was collected in an upright reflection mode using the same objective and imaged on a 100-m multimode fiber. This

fiber functions as confocal pinhole and entrance slit for guiding the Stokes scattered light into the spectrometer, which uses a 600-lpmm grating to disperse the light onto a –70°C cooled CCD camera (ANDOR iDus 401 BR-DD). All spectra were acquired over 30 averages with a 1.1-s integration time. In the waveguide coupled case, the objective and chip were aligned with a <100-nm precision based on a maximum intensity of SiN waveguide's Raman spectrum. Simultaneously, maximum light scattering along the waveguide was observed from a camera imaging the top-surface of the chip.

4.4 FDTD simulation

The 3D Lumerical FDTD simulation model was described in detail in our earlier work [24]. Briefly, we considered a 700-nm-wide by 200-nm-high SiN rib waveguide with a refractive index value of 1.9 on top of an SiO_2 substrate with index 1.45. The bowties are implemented as a stack of 2-nm Ti adhesion layer in between the SiN and a 30-nm Au layer, respectively modeled using the built-in CRC and Johnson & Christy models. A gold-bound monolayer of pNTP was represented by a 1-nm-thick layer with refractive index of 1.62 [38]. A mode source was used to launch the fundamental TE mode in the SiN strip waveguide, and the conversion efficiency of this mode to Stokes scattered light was calculated as described in the SI.

Acknowledgments: F.P. acknowledges the Bijzonder Onderzoeksfonds (BOF) from Ghent University. P.W. acknowledges the Research Foundation Flanders (FWO) for a predoctoral fellowship. R.B. acknowledges the ERC-advanced grant INSPECTRA.

References

[1] Yampolsky S, Fishman DA, Dey S, et al. Seeing a single molecule vibrate through time-resolved coherent anti-Stokes Raman scattering. Nat Photonics 2014;8:650–6.
[2] Ji-Xin C, Xie XS. Coherent Raman scattering microscopy. Boca Raton, USA, CRC Press, 2016.
[3] Anker JN, Hall WP, Lyandres O, Shah NC, Zhao J, Van Duyne RP. Biosensing with plasmonic nanosensors. Nat Mater 2008;7:442–53.
[4] Willets KA, Van Duyne RP. Localized surface plasmon resonance spectroscopy and sensing. Annu Rev Phys Chem 2007;58:267–97.
[5] Halas NJ, Lal S, Chang W-S, Link S, Nordlander P. Plasmons in strongly coupled metallic nanostructures. Chem Rev 2011;111:3913–61.
[6] Giannini V, Fernández-Domínguez AI, Heck SC, Maier SA. Plasmonic nanoantennas: fundamentals and their use in controlling the radiative properties of nanoemitters. Chem Rev 2011;111:3888–912.
[7] Chu Y, Banaee MG, Crozier KB. Double-resonance plasmon substrates for surface-enhanced Raman scattering with enhancement at excitation and Stokes frequencies. ACS Nano 2010;4:2804–10.
[8] Ye J, Wen F, Sobhani H, et al. Plasmonic nanoclusters: near field properties of the fano resonance interrogated with SERS. Nano Lett 2012;12:1660–7.
[9] Bontempi N, Carletti L, De Angelis C, Alessandri I. Plasmon-free SERS detection of environmental CO_2 on TiO_2 surfaces. Nanoscale 2016;8:3226–31.
[10] Gallinet B, Siegfried T, Sigg H, Nordlander P, Martin OJF. Plasmonic radiance: probing structure at the Angström scale with visible light. Nano Lett 2013;13:497–503.
[11] Siegfried T, Ekinci Y, Martin OJF, Sigg H. Gap plasmons and near-field enhancement in closely packed sub-10 nm gap resonators. Nano Lett 2013;13:5449–53.
[12] Li J, Chen C, Jans H, et al. 300 mm Wafer-level, ultra-dense arrays of Au-capped nanopillars with sub-10 nm gaps as reliable SERS substrates. Nanoscale 2014;6:12391–6.
[13] Seok TJ, Jamshidi A, Eggleston M, Wu MC. Mass-producible and efficient optical antennas with CMOS-fabricated nanometer-scale gap. Opt Express 2013;21:16561–9.
[14] Schlücker S. Surface-enhanced raman spectroscopy: concepts and chemical applications. Angewandte Chemie 2014;53:4756–95.
[15] Wuytens PC, Demol H, Turk N, et al. Gold nanodome SERS platform for label-free detection of protease activity. Faraday Discuss 2017;205:345–61.
[16] Alessandri I, Lombardi JR. Enhanced Raman scattering with dielectrics. Chem Rev 2016;116:14921–81.
[17] Benabid F, Knight JC, Antonopoulos G, Russell PSJ. Stimulated Raman scattering in hydrogen-filled hollow-core photonic crystal fiber. Science 2002;298:399–402.
[18] Dhakal A, Subramanian AZ, Wuytens P, Peyskens F, Le Thomas N, Baets R. Evanescent excitation and collection of spontaneous Raman spectra using silicon nitride nanophotonic waveguides. Opt Lett 2014;39:4025–8.
[19] Evans CC, Liu C, Suntivich J. TiO_2 Nanophotonic sensors for efficient integrated evanescent Raman spectroscopy. ACS Photonics 2016;3:1662–9.
[20] Stievater TH, Holmstrom SA, Kozak DA, et al. Trace-gas raman spectroscopy using functionalized waveguides. Optica 2016;3:891–6.
[21] Boerkamp M, van Leest T, Heldens J, et al. On-chip optical trapping and Raman spectroscopy using a TripleX dual-waveguide trap. Opt Express 2014;22:30528–37.
[22] Lin S, Zhu W, Jin Y, Crozier KB. Surface-enhanced Raman scattering with Ag nanoparticles optically trapped by a photonic crystal cavity. Nano Lett 2013;13:559–63.
[23] Kong L, Lee C, Earhart CM, Cordovez B, Chan JW. A nanotweezer system for evanescent wave excited surface enhanced Raman spectroscopy (SERS) of single nanoparticles. Opt Express 2015;23:6793–802.
[24] Peyskens F, Dhakal A, Van Dorpe P, Le Thomas N, Baets R. Surface enhanced Raman spectroscopy using a single mode nanophotonic-plasmonic platform. ACS Photonics 2016;3:102–8.

[25] Peyskens F, Subramanian AZ, Neutens P, et al. Bright and dark plasmon resonances of nanoplasmonic antennas evanescently coupled with a silicon nitride waveguide. Opt Express 2015;23:3088–101.
[26] Measor P, Seballos L, Yin D, et al. On-chip surface-enhanced Raman scattering detection using integrated liquid-core waveguides. Appl Phys Lett 2007;90:211107-1–211107-4.
[27] Wuytens PC, Skirtach AG, Baets R. On-chip surface-enhanced Raman spectroscopy using nanosphere-lithography patterned antennas on silicon nitride waveguides. Opt Express 2017;25:12926–34.
[28] Wang D, Zhu W, Best MD, Camden JP, Crozier KB. Directional Raman scattering from single molecules in the feed gaps of optical antennas. Nano Lett 2013;13:2194–8.
[29] Dhakal A, Wuytens P, Raza A, Le Thomas N, Baets R. Silicon nitride background in nanophotonic waveguide enhanced raman spectroscopy. Materials 2017;10:1–13.
[30] Weber-Bargioni A, Schwartzberg A, Schmidt M, et al. Functional plasmonic antenna scanning probes fabricated by induced-deposition mask lithography. Nanotechnology 2010;21:065306.
[31] Le Ru EC, Etchegoin PG. Quantifying SERS enhancements. MRS Bull 2013;38:631–40.
[32] Siegfried T, Ekinci Y, Martin OJF, Sigg H. Engineering metal adhesion layers that do not deteriorate plasmon resonances. ACS Nano 2013;7:2751–7.
[33] Peyskens F, Dhakal A, Van Dorpe P, Le Thomas N, Baets R. Hybrid single mode nanophotonic-plasmonic waveguides for on-chip surface enhanced Raman spectroscopy. The 7th International Conference on Metamaterials, Photonic Cyrstals and Plasmonics (META'16) 2016:424–5.
[34] Tabatabaei M, Sangar A, Kazemi-Zanjani N, Torchio P, Merlen A, Lagugné-Labarthet F. Optical properties of silver and gold tetrahedral nanopyramid arrays prepared by nanosphere lithography. J Phys Chem C 2013;117:14778–86.
[35] Wang W, Dong Z, Gu Y, et al. Giant photoluminescence enhancement in tungsten-diselenide-gold plasmonic hybrid structures. Nat Comm 2016;7:11283.
[36] Aouani H, Rahmani M, Navarro-Cía M, Maier SA. Third-harmonic-upconversion enhancement from a single semiconductor nanoparticle coupled to a plasmonic antenna. Nat Nanotech 2014;9:290–4.
[37] Hoang TB, Akselrod GM, Mikkelsen MH. Ultrafast room-temperature single photon emission from quantum dots coupled to plasmonic nanocavities. Nano Lett 2016;16:270–5.
[38] Jakubowicz A, Jia H, Wallace RM, Gnade BE. Adsorption kinetics of p-nitrobenzenethiol self-assembled monolayers on a gold surface. Langmuir 2015;21:950–5.

Supplemental Material: The online version of this article offers supplementary material (https://doi.org/10.1515/nanoph-2018-0003).